SIMULTANEOUS SOHO AND GROUND-BASED OBSERVATIONS OF A LARGE ERUPTIVE PROMINENCE AND CORONAL MASS EJECTION

S. P. PLUNKETT[1,*], A. VOURLIDAS[2], S. ŠIMBEROVÁ[3], M. KARLICKÝ[3], P. KOTRČ[3], P. HEINZEL[3], YU. A. KUPRYAKOV[4], W. P. GUO[5] and S. T. WU[5]

[1]*Universities Space Research Association, Naval Research Laboratory, Washington, DC 20375, U.S.A. (e-mail: plunkett@cronus.nrl.navy.mil)*

[2]*Center for Earth Observing and Space Research, Computational Sciences Institute, George Mason University, Fairfax, VA 22030, U.S.A.*

[3]*Astronomical Institute, Academy of Sciences of the Czech Republic, 25165 Ondřejov, Czech Republic*

[4]*Sternberg Astronomical Institute, 119899 Moscow, Russia*

[5]*Center for Space Plasma and Aeronomic Research and Department of Mechanical and Aerospace Engineering, The University of Alabama in Huntsville, Huntsville, AL 35899, U.S.A.*

(Received 13 September 1999; accepted 7 January 2000)

Abstract. Coronal mass ejections (CMEs) are frequently associated with erupting prominences near the solar surface. A spectacular eruption of the southern polar crown prominence was observed on 2 June 1998, accompanied by a CME that was well-observed by the LASCO coronagraphs on SOHO. The prominence was observed in its quiescent state and was followed throughout its eruption by the SOHO EIT and later by LASCO as the bright, twisted core of the CME. Ground-based Hα observations of the prominence were obtained at the Ondřejov Observatory in the Czech Republic. A great deal of fine structure was observed within the prominence as it erupted. The prominence motion was found to rotate about its axis as it moved outward. The CME contained a helical structure that is consistent with the ejection of a magnetic flux rope from the Sun. Similar structures have been observed by LASCO in many other CMEs. The relationship of the flux rope to other structures in the CME is often not clear. In this event, the prominence clearly lies near the trailing edge of the structure identified as a flux rope. This structure can be observed from the onset of the CME in the low corona all the way out to the edge of the LASCO field of view. The initiation and evolution of the CME are modeled using a fully self-consistent, 3D axisymmetric, MHD code.

1. Introduction

Coronal mass ejections (CMEs) are often observed in association with erupting prominences or disappearing filaments on the solar disk (Gosling *et al.*, 1974; Munro *et al.*, 1979; Sheeley *et al.*, 1983; Webb and Hundhausen, 1987, St. Cyr and Webb, 1991). CMEs are usually observed by coronagraphs, either on the ground or in space, as increased Thomson scattering of photospheric white light by coronal electrons. The morphology of many CMEs observed in this way consists of a three-part structure: a bright leading edge, dark cavity and a bright core or kernel (Illing

*Address for correspondence: Mail Code 682.3, NASA Goddard Space Flight Center, Greenbelt, MD 20771, U.S.A.

Solar Physics **194:** 371–391, 2000.
© 2000 *Kluwer Academic Publishers. Printed in the Netherlands.*

and Hundhausen, 1986). The bright core is often identified as cool, dense prominence material, although it is difficult to prove such an association from white-light coronal observations alone. The pre-CME coronal structure is frequently identified as a helmet streamer with a high-density dome, a low-density cavity and an embedded prominence at the base of the cavity (Low, 1994; Hundhausen, 1999). CMEs are also frequently associated with solar flares. In these cases, the CME and flare are believed to be different manifestations of a complex release of magnetic energy in the corona (e.g., Dryer *et al.*, 1998). The presence or absence of hard X-ray and radio burst signatures can be considered as a measure of the association between flares and CMEs. Typical flare signatures require the presence of substantial amounts of energetic particles. CMEs that occur without significant particle acceleration in the low corona are usually not accompanied by flare signatures.

It is well established that interplanetary magnetic clouds (Burlaga *et al.*, 1981) are associated with CMEs (Klein and Burlaga, 1982; Wilson and Hildner, 1984; Gosling, 1990). Gosling showed that perhaps $\frac{1}{3}$ of all interplanetary CMEs are magnetic clouds. Many magnetic clouds can be modeled as force-free magnetic flux ropes (Burlaga, 1988).

Magnetic clouds have also been associated with eruptive prominences (Bothmer and Schwenn, 1994; Rust, 1994). The precise relationship between the flux-rope geometry and the substructures within CMEs is not clear. Eruptive prominences often show helical features (Vršnak, Ruždjak, and Rompolt, 1991) suggestive of a flux-rope geometry. In some models (Anzer, 1978; Mouschovias and Poland; 1978) the leading edge of the CME is treated as a flux rope. Tsurutani and Gonzalez (1995) and Gopalswamy *et al.* (1998) argue that the magnetic flux rope that later becomes the interplanetary magnetic cloud is more likely to be contained in the low-density cavity above the prominence. Recently, Wood *et al.* (1999) presented two CMEs observed by the LASCO coronagraphs on SOHO on 23 February and 30 April 1997. The former CME was accompanied by a prominence eruption, while the latter had no apparent accompanying prominence. However, both CMEs were otherwise similar in appearance, having bright circular rims which were interpreted as marking the apexes of expanding magnetic ropes. The kinematic and morphological properties of these CMEs are in agreement with the models of Chen (1996) and Wu and Guo (1997a). Dere *et al.* (1999) presented further examples of helical structures in CMEs observed by LASCO, that they interpreted as flux ropes. A further study of the dynamics of several flux-rope CMEs has recently been performed (Vourlidas *et al.*, 2000).

In this paper, we present observations of a huge eruptive prominence and associated CME observed on 2 June 1998. We combine observations from the LASCO white-light and emission-line coronagraphs (Brueckner *et al.*, 1995) and the EIT (Delaboudinière *et al.*, 1995) on SOHO, with ground-based Hα telescope images and spectra from Ondřejov Observatory in the Czech Republic. We follow the evolution of the eruption from its onset at the solar surface out to a projected distance of 30 $R_{\odot}$. The key questions that are addressed by these observations

are: (1) What is the three-dimensional nature of the prominence motion? (2) How does the prominence structure observed in Hα and EUV spectral lines relate to the CME structures observed in broadband Thomson-scattered white light? (3) What is the morphological relationship between the flux rope and the prominence? And (4) Where and when does the flux rope form? (Is it present prior to eruption, or does it form in the corona as a result of the eruption, perhaps by reconnection in a sheared arcade?) We also investigate the evolution of the CME energy with time. The observational results are compared with the model predictions of Wu and Guo (1997a) to gain insight into the physical processes that drive the eruption.

2. Evolution of the Hα Prominence

The prominence was first observed in Hα on June 2, 1998 at about 06:00 UT, when regular observations started at Ondřejov. The prominence was observed above the southwest solar limb, about 15° south of active regions NOAA AR 8224 and AR 8228. Detailed analysis reveals that the prominence was oriented in the east-west direction and thus the observations show an interesting side view of this prominence.

The state of the Hα prominence at 06:14:21 UT, just at the beginning of the ejection process, is shown in Figure 1. The height of the prominence is about 150 000 km above the limb. The prominence is anchored in three places. The eastern part shows a helical structure and is anchored on the visible disk. The western part of this huge loop is anchored behind the limb. The central part shows a peaked 'V' structure and appears to be supported from below by faint loops, forming an X-point magnetic field configuration. These observations suggest that the prominence has the inverse polarity magnetic field topology (Kuperus and Raadu, 1974).

The ejection of this prominence started at about 06:00 UT with motions in the eastern leg of the prominence (see changes in the helical structure at 06:14:21 and 08:27:26 UT in Figure 1). We estimated the critical pitch angle ϑ of a helical thread as (Vršnak *et al.*, 1991):

$$\tan\vartheta = 2\pi r/\lambda; \quad \vartheta = 50^\circ ,$$

where r is the radius of 'coil' and λ is is the pitch length.

The eastern part of the prominence moves very rapidly upwards. Later on the western part also starts to move (09:19:32 UT, see Figure 1). Helical structures are visible throughout the entire prominence. The speed of the prominence increases with time and the Hα emission becomes fainter (see the image at 09:47:07 UT in Figure 1).

From 06:00 to about 09:00 UT the prominence was clearly visible in Hα and after that it becomes faint as it moves farther from the disk (about 2–3 $R_\odot$). The last useful image data are at 10:00 UT, when the prominence fades into the background. The raw image data were pre-processed by standard methods (noise

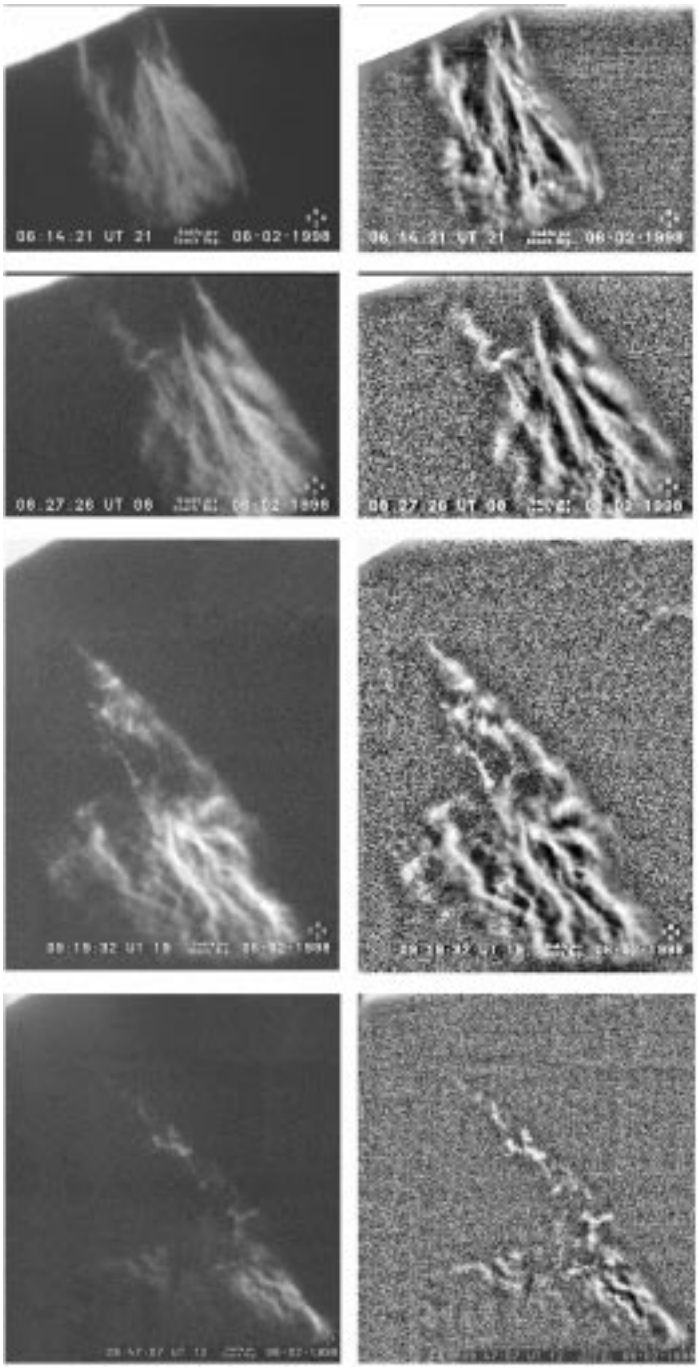

Figure 1. Prominence eruption on 2 June 1998 observed in Hα at the Ondřejov Observatory. The images in the left column have not had any special processing applied. The images in the right column have been processed to reveal the fine structure of the prominence. Time progresses from top to bottom in this figure. East is to the left and north is to the top in these images. The spatial scale in the last two pairs of images (09:19 UT and 09:47 UT) has been reduced from that in the earlier images by 80% and 50%, respectively.

removal, contrast stretching, background contrast equalization). The last two images in Figure 1 were processed further by treating the image in three overlapping parts, and combining the processed parts into a single image (Flusser, 1992).

The images in the right column of Figure 1 were further processed using a method of local optimization of density to reveal the fine details of the prominence structure. This is the only difference between the two columns in Figure 1. The image processing technique uses a modified form of histogram equalization mapping and was first developed by Šimberová and Suk (1993). The technique was applied to the analysis of large-scale coronal structures in soft X-ray images (Šimberová, Karlický, and Švestka, 1993). A new version of the method was introduced by Kotrč *et al.* (1998) to reveal fine structure in Hα images of prominences. The most important parameters are the size and shape of the sub-image that is used to perform the density transformation. The optimal sub-image was chosen according to the results of numerical experiments in Kotrč, Korčáková, and Kupryakov (1998). The optimal shape in this case is an ellipse with the major axis inclined along the direction of motion of the prominence. The size of the sub-image depends on the size of the patterns we need to recognize. For this reason, the major radius of the sub-image was chosen as 40 pixels, with the ratio of semi-axes chosen to be $\frac{4}{3}$.

During a substantial part of its active development, the prominence was observed using the Multichannel Flare Spectrograph. Hα spectra and slit-jaw filtergrams of the eruptive prominence were registered by a system of videocameras with a high temporal resolution of 25 images per second (Kotrč, 1997). The prominence intensity became rather weak during the later phases of the eruption when the prominence was more than 1 $R_\odot$ above the SW limb, and consequently the signal-to-noise ratio was low. This circumstance, however, should not influence the estimation of Doppler velocities as the individual profiles are well defined. The spectra were digitized and processed to derive Doppler velocity components of both the bulk translational and rotational motion of the prominence plasma. We used an IDL 'curve-fit' procedure to do a Gaussian fit to the measured line profiles and to locate the wavelength λ at line center. The Doppler line-of-sight velocity component v_l is then evaluated from the equation

$$v_l = c\frac{\lambda - \lambda_0}{\lambda_0} ,$$

where c is the velocity of light, λ_0 is the reference wavelength and λ is the center of the Gaussian profile evaluated for each position along the slit.

Three Hα spectra corresponding to different positions of the spectrograph slit on the prominence body observed between 09:48–09:51 UT were obtained. The slit-jaw image and spectrum at 09:51 UT are shown in Figure 2 and the evaluated Doppler velocity components for each position on the slit can be seen in Figure 3. An inclined linear pattern with the same inclination angle can be seen at each position and we interpret this as evidence for rotation of the prominence plasma about its central axis in all the Hα spectra. The inclined linear pattern in each case

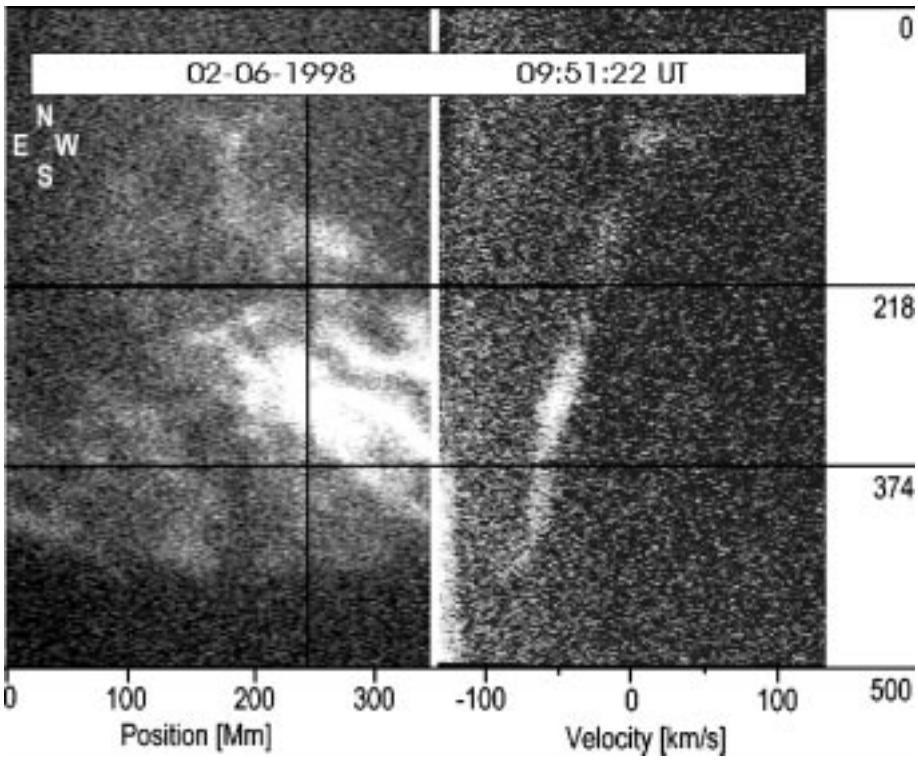

Figure 2. A slit-jaw picture of the eruptive prominence is on the left-hand side; the corresponding Hα spectrum is on the right-hand side. The solar limb is at the upper left corner. The vertical line marks the spectrograph slit. Numbers on the vertical scale denote positions along the slit in Mm. Two horizontal lines mark hairs on the slit.

is shifted with respect to the velocity zero value. This pattern can not be explained only in terms of a simple rotational motion, but requires a bulk translational component as well. For evaluation of the rotational velocities from such a linear and asymmetrical pattern, we constructed a simple model of a rotating prominence having also a line-of-sight constant bulk velocity component. When such a cylindrical prominence (the axis of which crosses the spectrograph slit) rotates and in addition moves relative to the observer with a bulk velocity v_t, then the resulting Doppler velocity components produce the observed linear and asymmetrical pattern. The resulting measured line-of-sight velocity v_l can be expressed as

$$v_l = v_t + v_r \ .$$

By matching both v_t and v_r of the cylinder one can find the best approximation to the rotational pattern of the spectrum. Then from simple geometrical considerations based on symmetry, and taking into account the minimum and maximum limits of the Doppler velocities components (see Figure 3), we can estimate the rotation and translation velocities in the period 09:48–09:51 UT. The appearance

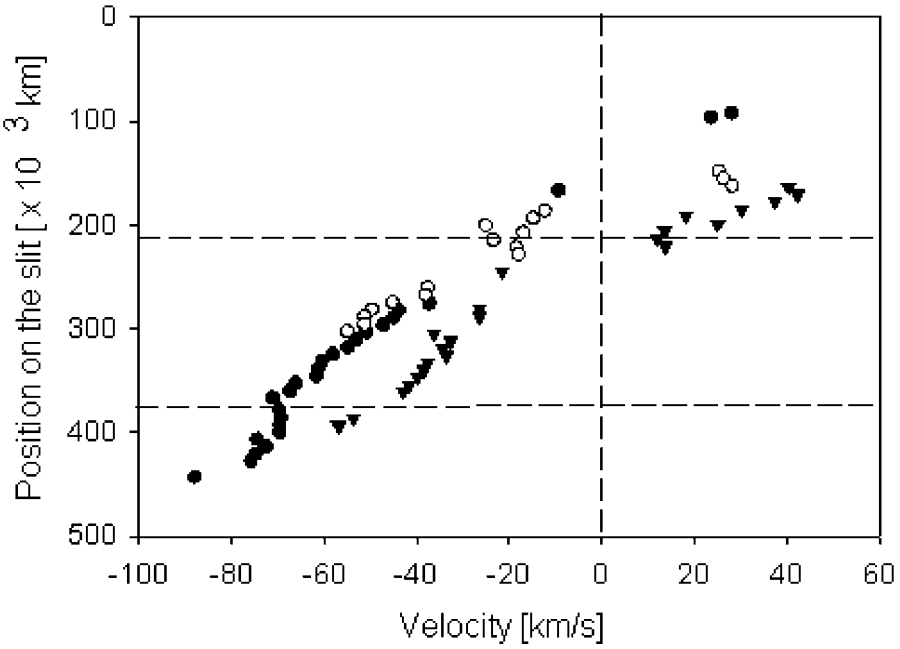

Figure 3. Doppler (line-of-sight) velocities derived from Hα spectra at three locations on the prominence at 09:48:40 UT (open circles), 09:48:52 UT (closed circles) and 09:51:52 UT (triangles). The Doppler velocity components of all the three processed prominence scans display an inclined pattern that can be explained as a result of rotating structures.

of the spectra at other times is very similar. The radius of the prominence cylinder is estimated as $r = 170\,000$ km, $\omega = 0.0004$ rad s^{-1}, i.e., the amplitude of the rotational velocity component v_r reaches 70 km s^{-1} and the additional bulk velocity component $v_t = -20$ km s^{-1} (the signs $\pm$ are used to denote the directions away from/towards the observer). Thus we conclude that the prominence motion is a combination of rotation about its axis and a bulk motion towards the observer.

3. EIT Observations of the Prominence

The prominence that erupted on 2 June 1998 was part of an extended polar crown filament channel that was visible on the solar disk for at least the previous half rotation. The filament channel is visible in Figure 4 as a dark lane in EIT images taken in the Fe XII emission line at 195 Å, (peak temperature of emission about 1.5×10^6 K). The feet of the overlying coronal arcade can be seen in the Fe XII images as bright narrow ribbons on either side of the dark filament channel. The arcade is visible in EIT images taken in hotter emission lines, for example Fe XV 284 Å, and in broadband *Yohkoh* Soft X-ray Telescope (SXT) images.

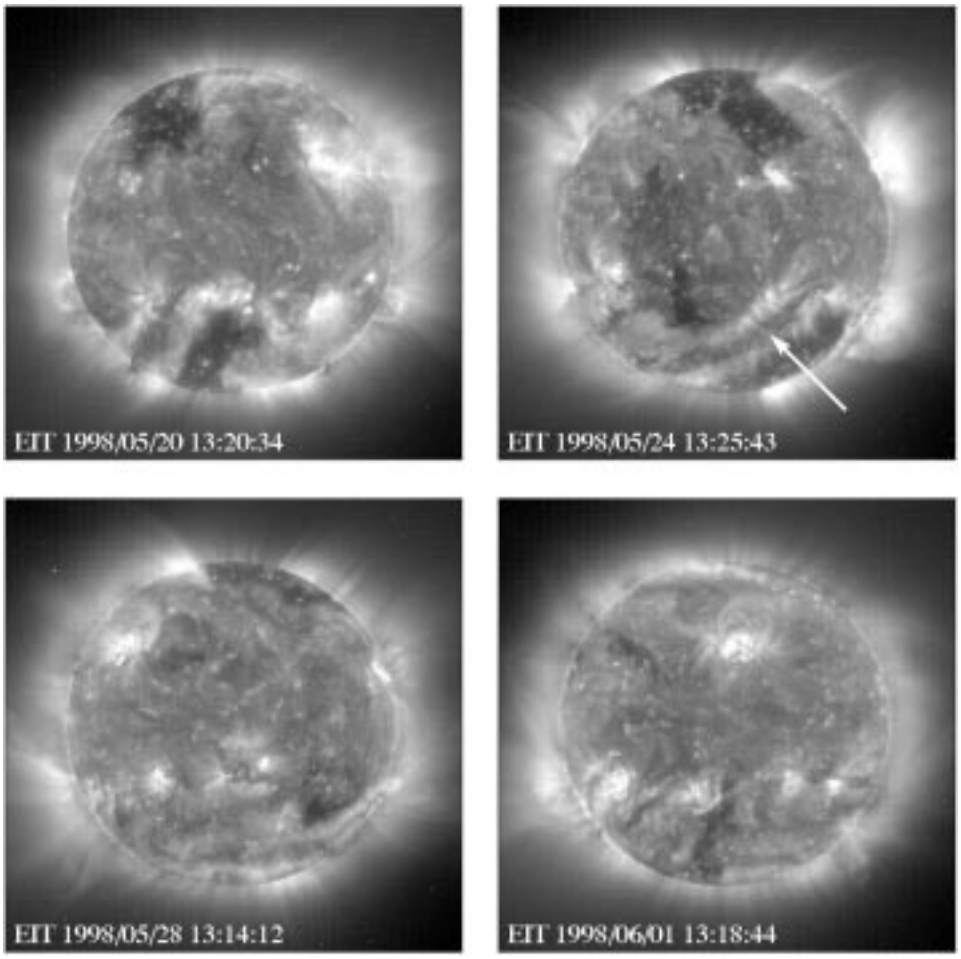

Figure 4. EIT 195 Å images during the solar rotation prior to 2 June showing the extended dark filament (indicated by the white arrow) as it rotates across the disk.

The eruption of this prominence was well observed by EIT. Images in the Fe XII 195 Å line were obtained every 15 minutes during 1 June and 2 June, and images in the other three EIT lines (He II 304 Å, Fe IX/X 171 Å, and Fe XV 284 Å) were taken every 6 hours. Early on 1 June, a dark prominence was clearly seen in the Fe XII images, projected on the brighter coronal background characteristic of plasma near 1.5×10^6 K. Such absorption features are frequently seen in hot EIT lines and usually correspond to much cooler structures that are visible as emission features in the He II 304 Å line (peak temperature of emission 8.0×10^4 K) – see for example Figure 2 in Moses *et al.* (1997). The generally accepted interpretation of these features is that cool structures absorb the background coronal emission at wavelengths corresponding to H I, He I and He II continua (Kucera, Andretta, and Poland, 1998).

The northern end of the prominence began to brighten and parts of the structure appeared in emission at 195 Å at about 06:00 UT on 1 June. This was the first evidence for activation of this prominence, which had otherwise been quiescent during its passage across the solar disk. Following this activation, a horn-shaped structure became visible at the top of the prominence. This feature appears qualitatively similar to the concave shape expected for the trailing edge of a flux rope suspended in a streamer cavity overlying the prominence (Low, 1994). It is unclear whether this structure already existed but only became visible following the prominence activation, or whether it was formed in the corona as a result of the activation process. In either case, it was clearly present many hours before the prominence erupted.

At about 05:00 UT on 2 June, the prominence lost its equilibrium and began to rise. The first motions appeared in the northern part of the prominence. The eruption of the prominence is shown in Figure 5. The left column in this figure shows a sequence of EIT 195 Å images, unprocessed except for flat-fielding and dark current corrections. The right panel shows the same images with a suitable background subtracted to enhance the visibility of faint features. The concave-outward feature that we interpret as a flux rope is clearly visible in these processed images. The correspondence of features in the EIT and Hα images at various stages of the eruption was checked by visual inspection of near-simultaneous images that were overlaid on a computer screen. A very good correspondence between the bright features in Hα and the dark features on the EIT 195 Å images was found (compare Figures 1 and 5). As the prominence rose higher into the corona, the overlying concave-outward structure expanded outwards with it. Beginning at about 10:30 UT, the base of the ejected structure became narrower, and post-ejection loops were formed on the limb beneath the location of the prominence. These loops, which presumably indicate magnetic field reconnection in the post-eruption streamer, continued to grow for many hours afterwards.

4. CME Observations

4.1. Morphology and kinematics of the CME

The CME that accompanied the prominence eruption was well observed by all three LASCO telescopes. Figure 6 shows the evolution of the event in C1. This figure shows a series of running difference images (i.e., each image shows the changes in coronal brightness from the preceding image; white indicates areas of increased brightness, while black indicates a decrease in brightness) taken in the green Fe XIV coronal emission line, with a peak emissivity at about 1.9×10^6 K. The leading edge of the CME is visible as a relatively faint and featureless loop-like structure at a projected height of about 2 $R_\odot$, at 07:40 UT. The CME core is visible as a bright, apparently twisted, structure trailing the leading edge in the

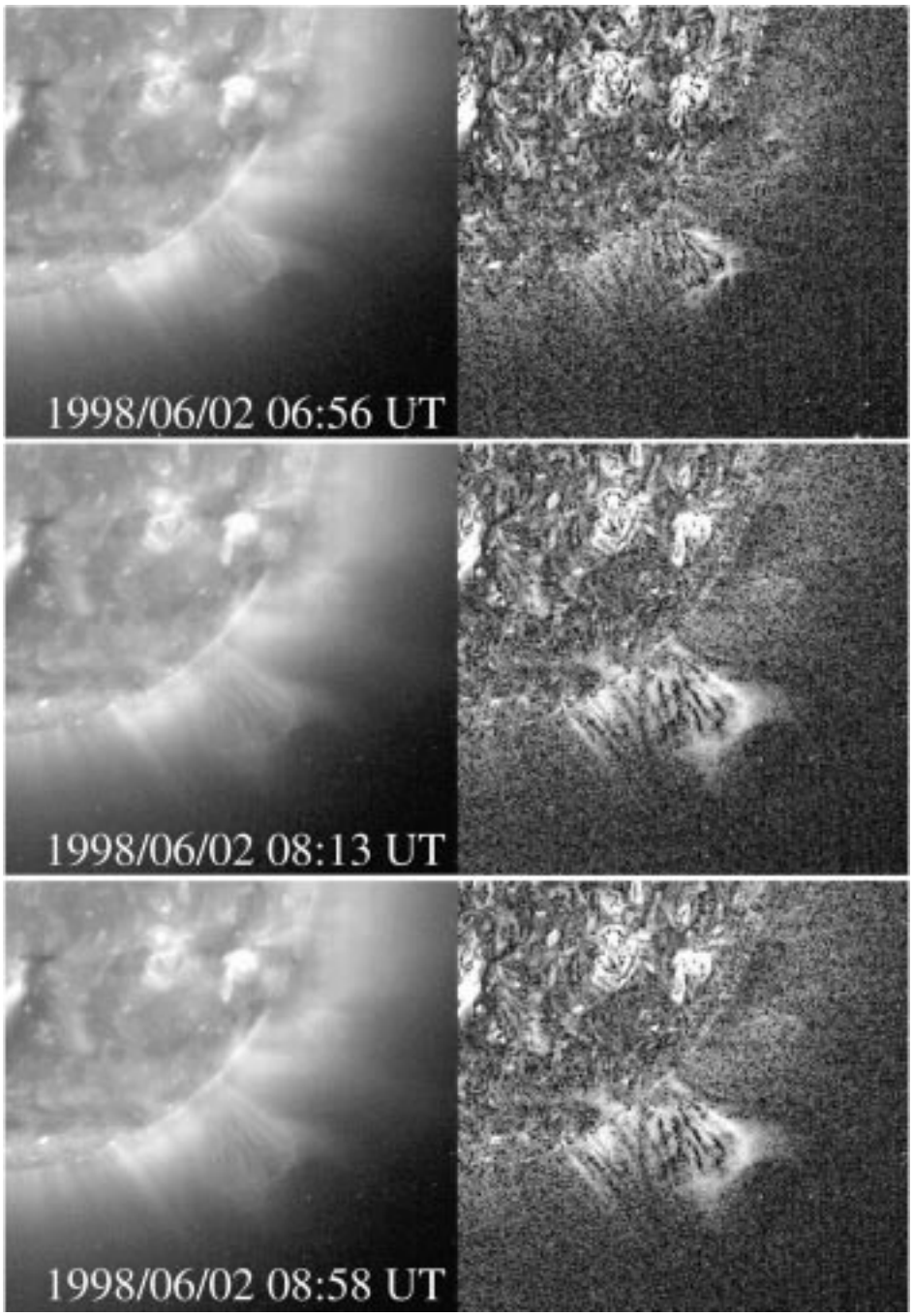

Figure 5. The eruption of the prominence on June 2 as observed in the EIT bandpass centered at 195 Å. The images in the right column have been processed to enhance the visibility of faint features.

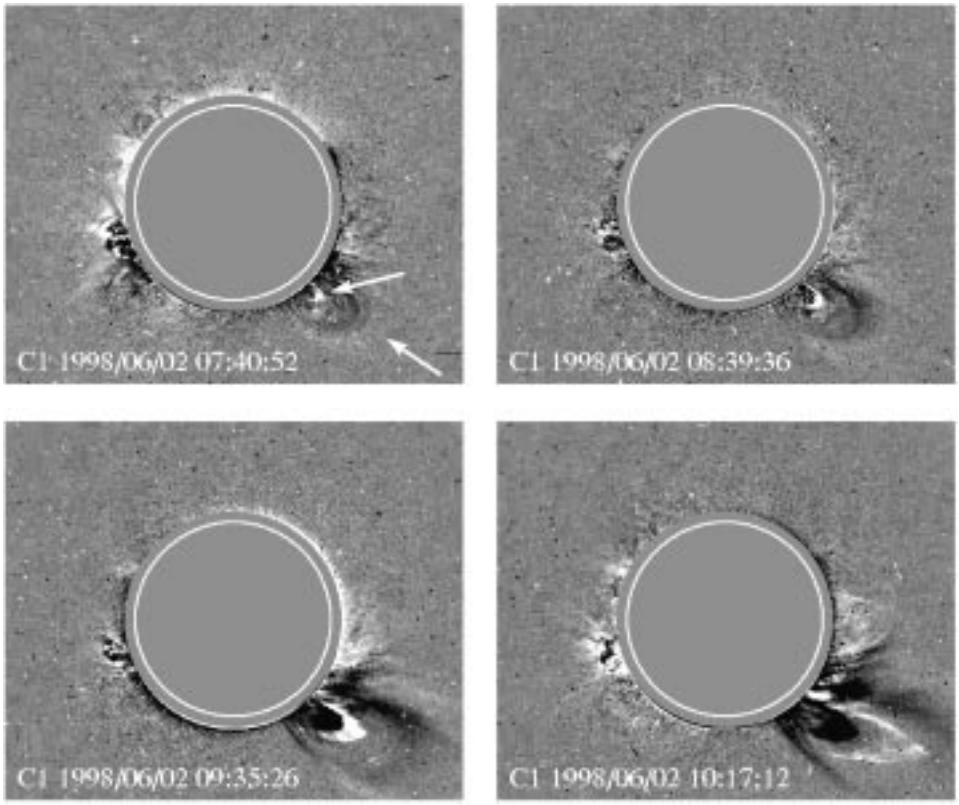

Figure 6. A series of running difference images in the Fe XIV green coronal line from LASCO C1, showing the CME and prominence eruption. The arrows mark the leading edge of the CME and the top of the prominence core.

same image. The fine structure of the core is clearly seen at 09:35 UT. The top of the core has a sharp V-shaped appearance at 10:17 UT, and much of the twisted structure visible in the earlier images appears to have 'unwound' at this time.

Figure 7 shows the evolution of the CME in C2. The loop-like leading edge and highly-structured core that were visible in C1 are seen here in Thomson-scattered broadband white light. The streamer that overlay the prominence prior to eruption was observed to swell for several hours below the cusp, located at a projected distance of about 4 $R_{\odot}$, before erupting as a CME. The leading loop is clearly visible in the C2 field of view at 09:37 UT, and the bright core appears in the next image, taken at 10:29 UT. The C2 image at 11:27 UT shows a very similar structure to that seen by C1 at 10:17 UT. A series of concave-outward, bright striations are visible near the top of the core in these images, and these striations move outward as a part of the overall CME structure. They appear to connect with the leading edge of the CME to form a closed, almost circular, structure. Similar structures have been reported in other CMEs observed by LASCO (Chen *et al.*, 1997; Wood

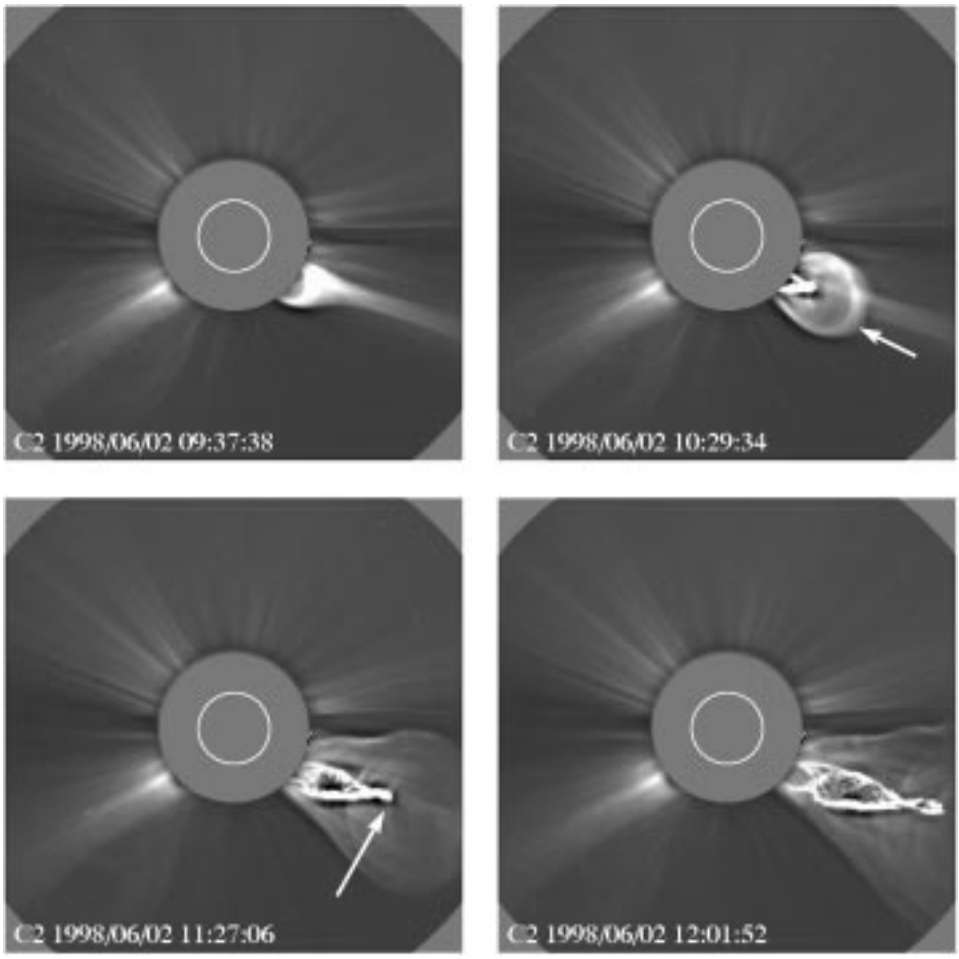

Figure 7. The CME and prominence eruption in white light, as observed by LASCO C2. The arrows mark the leading edge of the CME and the top of the prominence core.

et al., 1999; Dere *et al.*, 1999; Vourlidas *et al.*, 2000), and have been interpreted as evidence for a helical magnetic flux rope as part of the CME. The bright circular rim is interpreted as the boundary of the flux rope, with the main body of the flux rope lying within the CME cavity. The bright front may also be due, at least in part, to material that is piled up ahead of the flux rope as it expands outward. C3 images show that the same well-organized structure (featureless loop-like leading edge, circular striations and structured core) remains intact as the CME propagates into the outer corona, and that the entire structure remains connected back beneath the occulting disk by bright 'legs' that delineate the edges of the CME.

The radio spectral observations by the Ondřejov and Tremsdorf radiospectrographs show that the 2 June, 1998 CME can be considered as a 'radio silent' phenomenon. A noise storm of type I bursts in the 130–350 MHz frequency range

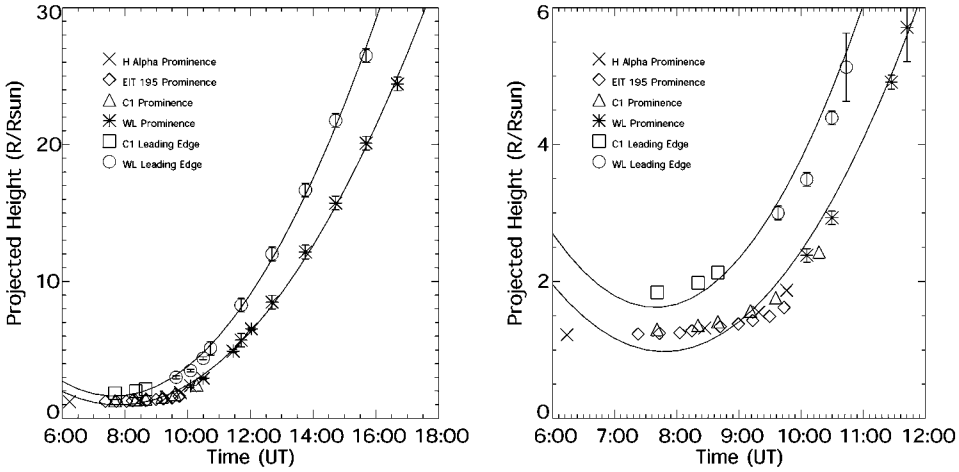

Figure 8. Height vs time plot showing the trajectory of the features marked with arrows in Figures 6 and 7, as well as the top of the prominence in Hα and in EIT. The solid curves represent the best fit to the data points, assuming constant acceleration for each feature. The right panel shows only the early stages of the eruption.

was observed between 06:00–08:40 UT. This noise storm is an indication of the equilibrium loss of the prominence and the start of the CME.

Figure 8 shows the trajectory of selected features within the CME as a function of time. The features that are plotted on these height-time curves are marked on the images in Figures 6 and 7, and represent the leading edge of the CME and the top of the bright core, respectively. The individual points were measured by following a time-lapse sequence of images on a computer screen, and marking the location of each feature in successive frames. The error bars represent conservative estimates of the measurement errors for each telescope using this technique. The trajectories of the prominence seen in EIT and in Hα are also plotted. Several points can immediately be deduced from these curves:

– All parts of the CME gradually accelerate from relatively slow speeds in the low corona all the way to the edge of the C3 field of view at a projected distance of 30 $R_{\odot}$. The assumption of constant acceleration is not a very good fit to the motion of the prominence close to the Sun, as can be seen from the right panel of Figure 8. The prominence travels with a constant projected velocity of about 20 km s^{-1} until it reaches a projected height of about 1.5 $R_{\odot}$, where it starts to accelerate. The leading edge accelerates more rapidly than the trailing portions, reaching a speed of about 1300 km s^{-1} before it leaves the C3 field of view. The CME core, in contrast, only reaches a speed of about 1000 km s^{-1} at the same radial distance.

– The prominence in Hα and EIT matches very well with the CME core observed in white light. This result, while not unexpected, confirms that the bright, highly structured core is indeed the same cool prominence material that was observed to erupt in the low corona.

– The concave-outward structure that lay near the top of the prominence in EIT prior to the eruption matches very well with the trailing edge of the structure identified as a helical flux rope in LASCO. This structure accelerates outward at a rate between that of the leading edge and the prominence core, such that the entire CME structure expands in the radial direction as it propagates outward.

4.2. FLUX ROPE ENERGETICS

Vourlidas *et al.* (2000) analyze the energetics of 11 LASCO CMEs that have clear flux rope morphology. The CME in this study is also part of their sample. Their measurements of potential, kinetic and magnetic energies are shown in Figure 9. They also derive a flux rope mass of 3×10^{16} g and a final speed of 900 km s^{-1}. The reader is referred to Vourlidas *et al.* (2000) for the details of the calculations. Figure 9 shows that the total energy of the flux rope is dominated by its kinetic and gravitational energies, and that the magnetic energy carried by the flux rope is significantly less than these two components. The magnetic energy also decreases by about an order of magnitude within the first few solar radii. This magnetic energy is given up to increased gravitational and kinetic energy, and in this sense one can say that the flux rope eruption is 'magnetically driven'. The gravitational energy dominates at radial distances less than about 12 $R_\odot$, after which the kinetic energy dominates. The total energy increases slightly with time, implying that there is a small, but significant, driving force acting on the flux rope. We suggest, although we cannot prove, that this force might come from the unwinding of the prominence magnetic field that is apparent in the changing structure of the prominence with radial distance in Hα, EIT, and C1 images.

5. CME Modeling

To understand the physical processes that drive this CME, we have employed a streamer and flux rope MHD model (Wu and Guo, 1997a) to simulate the eruption. This model was chosen because the observations indicate that the pre-event corona consists of a magnetic topology closely resembling the streamer and flux rope model. It is also known that magnetic flux emergence can drive fast CMEs (Wu and Guo, 1997b). The emergence of the magnetic flux can cause an increase of axial current in the flux rope, thus introducing an additional Lorentz force ($\mathbf{J} \times \mathbf{B}$) which destabilizes the streamer to launch a CME. This event is a fast CME (over 1000 km s^{-1}) and hence we use magnetic flux emergence as our driver mechanism for this event. To initiate our simulation, we take the initial state as given by Wu and Guo (1997a) by introducing an additional component of magnetic field (B_ϕ):

$$B_\phi^{n+1} = B_\phi^n \left[1 + \delta \left[1 - \frac{r^*}{0.85 r_f}\right]\right]$$

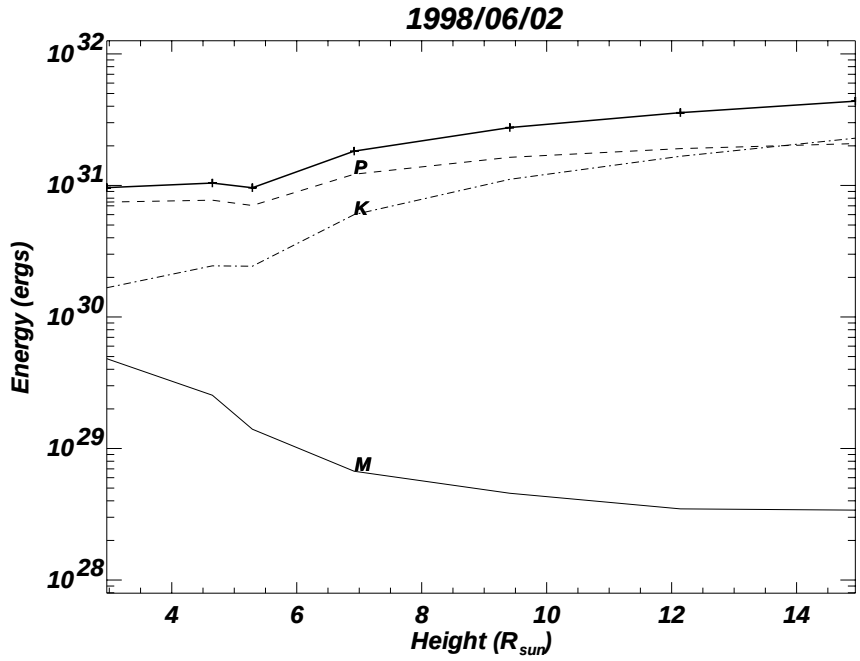

Figure 9. Evolution of the flux rope energy with height. The dashed line shows the gravitational potential energy, the dot-dashed line shows the kinetic energy, and the solid line shows the magnetic energy. The heavy solid line shows the sum of all three components.

as given by Equation (1) in Wu and Guo (1997a), where r_f is the radius of the flux rope, r^* is the distance between the center of the flux rope and where the strength of B_ϕ is raised, and δ is a parameter related to the magnitude of the increased field strength, which is chosen to be 0.006 for this case. In this case, we have to maintain the B_ϕ increase during the period of the simulation to reach the speed of the observed CME as shown in Figure 8. By examining Figure 10, it is easy to see that the center of the flux rope starts to move before the appearance of the CME. Here, we consider the front edge of the flux rope to represent the CME, because the helmet dome is ahead of the flux rope. These features can be seen from the evolution of the magnetic field and velocity and density plots in Figure 11. To mimic the observed white-light image, we have constructed the polarization brightness (pB) by integrating the computed density distribution along the line of sight as shown in Figure 12.

The results of this simulation are in good agreement with the observed kinematic and morphological properties of the CME, and thus we interpret this event as being due to the flux rope destabilization of the streamer to launch the CME. Note that the model does not explicitly contain a prominence as part of the pre-event structure.

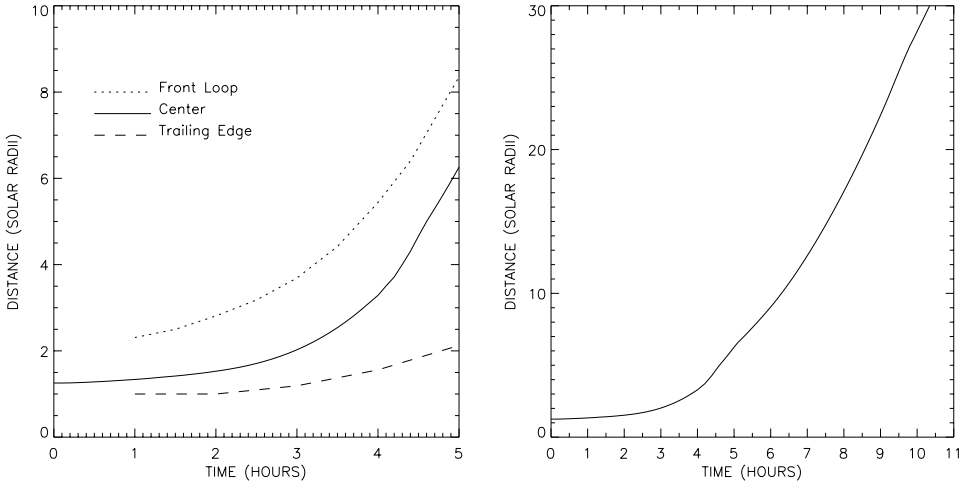

Figure 10. Height vs time plot for the CME frontal loop, center and trailing edge of the flux rope from the MHD model calculation. The left panel shows all three features out to a radial distance of 10 $R_\odot$, while the right panel shows the flux rope center out to 30 $R_\odot$.

6. Conclusions

We have presented detailed observations of a spectacular prominence eruption and associated CME, and have interpreted the observations using a self-consistent MHD model of an erupting helmet streamer and magnetic flux rope system. The prominence was part of a large polar crown filament structure that persisted for at least two weeks prior to eruption on 2 June 1998, and was tracked across the solar disk during this time by the SOHO EIT and ground-based instruments. Following the emergence of new magnetic flux into the corona on 1 June, a concave-outward structure could be observed in the low corona, located near the top of the prominence. This structure and the overlying coronal helmet streamer erupted outward the next day as part of a CME with a classical three-part structure, consisting of a leading loop-like feature, a low-density cavity which we interpret as a flux rope and the trailing prominence. The concave-outward feature observed in EIT is identified with similar striations observed at the trailing edge of the cavity in LASCO. A key result of these observations is that the structure that we interpret as a flux rope existed in the low corona prior to the onset of the CME, and was not formed as a result of the eruption, as some models would suggest (e.g., Gosling, 1990). It is difficult to tell from the observations precisely at what stage of the pre-CME evolution of the streamer and prominence system the flux rope was formed.

By combining ground-based Hα observations with the SOHO EIT and LASCO data, we have shown that the prominence structure observed in Hα matches very well with that seen in the other wavebands. In particular, the fine structure of the prominence matches very well between the Hα and EUV observations, with bright emission features in Hα corresponding closely with dark absorbing features in

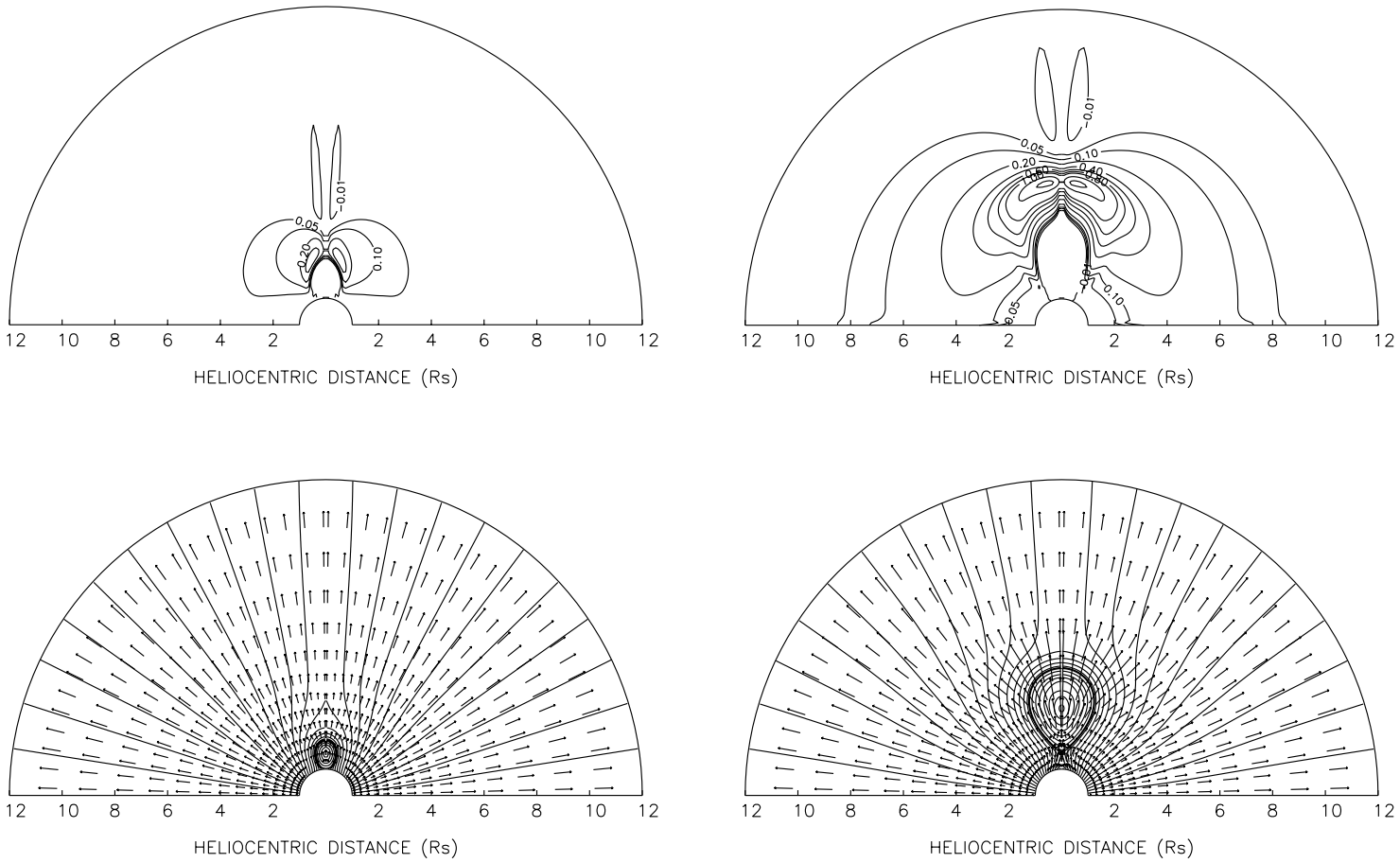

Figure 11. Modeled magnetic field line and velocity field (*bottom*) and relative density contours (*top*) at two and four hours following initiation of the CME.

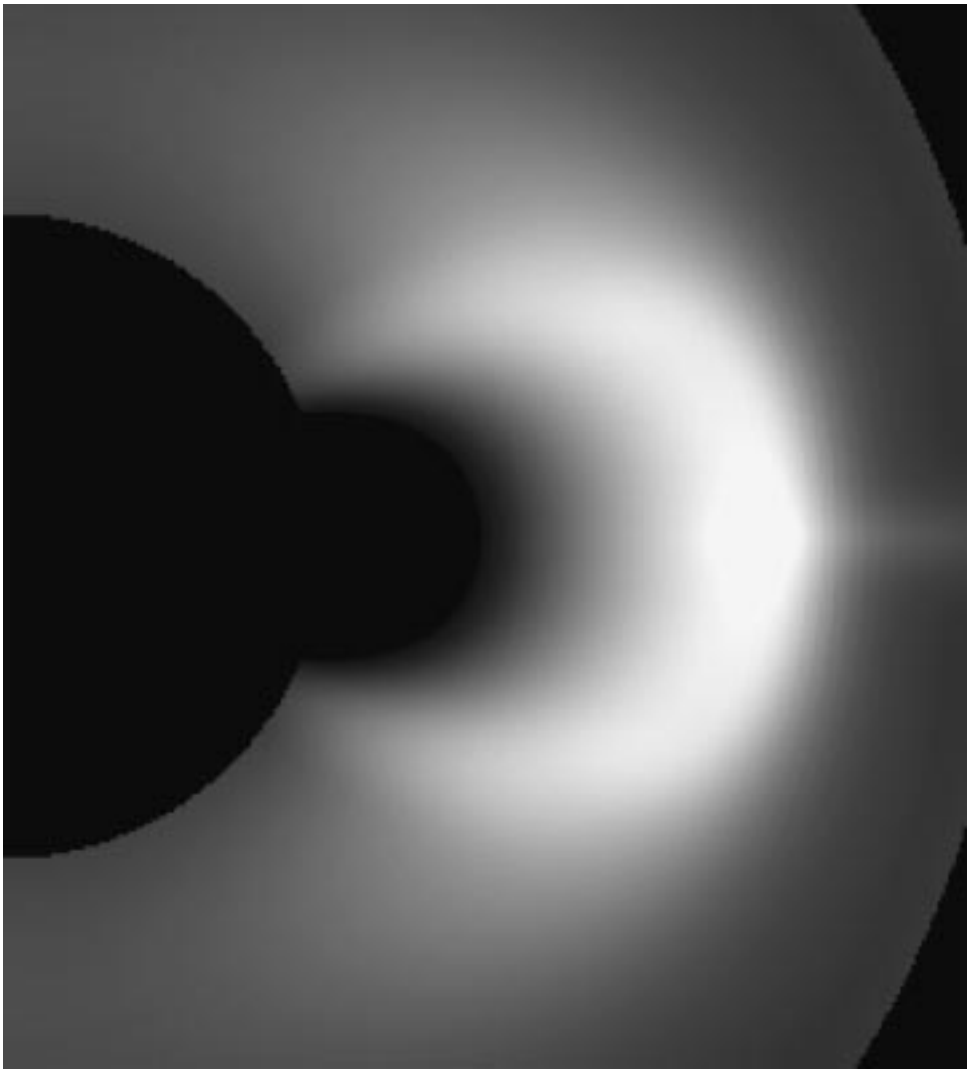

Figure 12. Line-of-sight integration of electron density from the MHD model calculation at two hours following initiation of the CME. The field of view closely matches that of LASCO C2 (2.2–6.5 $R_{\odot}$).

the Fe XII 195 Å coronal emission line. This correspondence in structural features persists as the prominence erupts. Furthermore, by following the trajectory of the erupting prominence through the LASCO field of view to a projected distance of 30 $R_{\odot}$, we have been able to show conclusively that the bright core of the CME observed in white light in the outer corona in fact corresponds to the Hα and EUV prominence observed lower in the atmosphere prior to and during eruption. The prominence core accelerates more slowly than the leading edge of the CME, and therefore is very unlikely to be the main driver of eruption. Rather, the prominence

eruption is more likely to be a consequence of the destabilization of the overlying coronal helmet streamer system caused by an increase in the magnetic strength of the embedded flux rope. Doppler measurements from Hα spectra show that the prominence plasma rotates about the central axis as it erupts outward, indicating that the prominence has a significant degree of helical twist in its structure.

The observations clearly show that the helmet streamer, cavity and prominence erupt outward as a single, organized magnetic structure. The bright front of the CME is identified as the leading edge of a helical magnetic flux rope, and the main body of the flux rope, with its high magnetic field strength, is identified with the low-density cavity. The dense prominence is located near the trailing edge of the flux rope structure. In other CMEs, the prominence sometimes appears embedded within the flux rope, but always near the trailing edge. Thus these observations support the conclusions of Tsurutani and Gonzalez (1995) and Gopalswamy *et al.* (1998) that the interplanetary structures known as magnetic clouds should be identified with the CME cavity, and not with the leading edge or the prominence.

The kinematic and morphological properties of the CME can be successfully reproduced with the self-consistent MHD model of Wu and Guo (1997a). This is a $2\frac{1}{2}$D (i.e., 3D axisymmetric geometry) model that describes the response of a coronal helmet streamer to the emergence of a helical magnetic flux rope. The CME is initiated by increasing the magnetic strength (azimuthal electric current) of the flux rope. This model has been used previously to interpret other CMEs observed by LASCO (e.g., Wu and Guo, 1997b). The model successfully describes the global properties of this particular CME, even though it does not contain a prominence structure. This again supports the conclusion that the prominence is not the major driving force behind the CME, and instead simply follows along when the overlying coronal structure erupts.

Measurements of CME energetics show that the total energy increases slightly with time and/or radial distance. Thus there must be a small but significant driving force that continues to supply energy to the CME as it propagates outward. We speculate that this force might come from unwinding of the prominence magnetic field behind the CME. Some support for this suggestion is found in the changing morphology of the prominence with time. However, this is a topic that clearly requires more work and further study of other events before it can be properly understood.

Acknowledgements

SPP is supported by NASA grant NAG5-8116. WPG and STW are supported by NASA Grant NAG5-6174 and NSF Grant ATM-9633629. Work in the Czech Republic was supported by the Grant Agency of the Academy of Sciences of the Czech Republic through Grant Nos. A3003707 and A3003902. We would like

to thank T. Vaněk and M. Knížek for their assistance during the observations at Ondřejov.

References

Anzer, U.: 1978, *Solar Phys.* **57**, 111.
Bothmer, V. and Schwenn, R.: 1994, *Space Sci. Rev.* **70**, 215.
Brueckner, G. E. and 14 co-authors: 1995, *Solar Phys.* **162**, 357.
Burlaga, L. F.: 1988, *J. Geophys. Res.* **93**, 7217.
Burlaga, L. F., Sittler, E., Mariani, F., and Schwenn, R.: 1981, *J. Geophys. Res.* **86**, 6673.
Chen, J.: 1996, *J. Geophys. Res.* **101**, 27499.
Chen, J., Howard, R. A., Brueckner, G. E., Santoro, R., Krall, J., Paswaters, S. E., St. Cyr, O. C., Schwenn, R., Lamy, P., and Simnett, G. M.: 1997, *Astrophys. J.* **490**, L191.
Delaboudinière, J.-P. and 27 co-authors: 1995, *Solar Phys.* **162**, 291.
Dere, K. P., Brueckner, G. E., Howard, R. A., Michels, D. J., and Delaboudinière, J.-P.: 1999, *Astrophys. J.* **516**, 465.
Dryer, M. and 23 co-authors: 1998, *Solar Phys.* **181**, 159.
Flusser, J.: 1992, *Pattern Recognition* **25** (1), 45.
Gopalswamy, N. and 11 co-authors: 1998, *Geophys. Res. Lett.* **25**, 2485.
Gosling, J. T.: 1990, in C. T. Russell, E. R. Priest and L. C. Lee (eds.), *Geophysical Monograph 58: Physics of Magnetic Flux Ropes*, American Geophysical Union, Washington, DC, p. 343.
Gosling, J. T., Hildner, E., MacQueen, R. M., Munro, R. H., Poland, A. I., and Ross, C. L.: 1974, *J. Geophys. Res.* **79**, 4581.
Hundhausen, A. J.: 1999, in K. T. Strong, J. L. R. Saba, B. M. Haisch and J. T. Schmelz (eds.), *The Many Faces of the Sun: Scientific Highlights of the Solar Maximum Mission*, Springer-Verlag, New York, p. 143.
Illing, R. M. E. and Hundhausen, A. J.: 1986, *J. Geophys. Res.* **91**, 10951.
Klein, L. W. and Burlaga, L. F.: 1982, *J. Geophys. Res.* **87**, 613.
Kotrč, P.: 1997, *Hvar Obs. Bull.* **21**, 97.
Kotrč, P., Korčáková D., and Kupryakov, Yu. A.: 1998, in A. Hanslmeier and M. Messerotti (eds.), *Astrophysics and Space Science Library 239, Motions in the Solar Atmosphere*, Kluwer Academic Publishers, Dordrecht, Holland, p. 379.
Kucera, T. A., Andretta, V., and Poland, A. I.: 1998, *Solar Phys.* **183**, 107.
Kuperus, M. and Raadu, M. A.: 1974, *Astron. Astrophys.* **31**, 189.
Low, B. C.: 1994, *Phys. Plasmas* **1**, 1684.
Moses, D. *et al.*: 1997, *Solar Phys.* **175**, 571.
Mouschovias, T. Ch. and Poland, A. I.: 1978, *Astrophys. J.* **220**, 675.
Munro, R. H., Gosling, J. T., Hildner, E., MacQueen, R. M., Poland, A. I., and Ross, C. L.: 1979, *Solar Phys.* **61**, 201.
Rust, D. M.: 1994, *Geophys. Res. Lett.* **21**, 241.
St. Cyr, O. C. and Webb, D. F.: 1991, *Solar Phys.* **136**, 379.
Sheeley, N. R., Jr., Howard, R. A., Koomen, M. J., and Michels, D. J.: 1983, *Astrophys. J.* **272**, 349.
Šimberová, S. and Suk, T.: 1993, *Lecture Notes Comp. Sci.* **719**, 759.
Šimberová, S., Karlický, M., and Švestka, Z.: 1993, *Solar Phys.* **146**, 343.
Tsurutani, B. T. and Gonzalez, W.: 1995, *J. Atmos. Terr. Phys.* **57**, 1369.
Vourlidas, A., Subramanian, P., Dere, K. P. and Howard, R. A.: 2000, *Astrophys. J.*, in press.
Vršnak, B., Ruždjak, V., and Rompolt, B.: 1991, *Solar Phys.* **136**, 151.
Webb, D. F. and Hundhausen, A. J.: 1987: *Solar Phys.* **108**, 383.
Wilson, R. M. and Hildner, E.: 1984, *Solar Phys.* **91**, 169.

Wood, B. E., Karovska, M., Chen, J., Brueckner, G. E., Cook, J. W., and Howard, R. A.: 1999, *Astrophys. J.* **512**, 484.

Wu, S. T. and Guo, W. P.: 1997a, in N. Crooker, J. Jocelyn and J. Feynman (eds.), *Geophysical Monograph 99: Coronal Mass Ejections*, American Geophysical Union, Washington, DC, p. 83.

Wu, S. T. and Guo, W. P.: 1997b, *Adv. Space Res.* **20** (12), 2313.